Biochemical properties of a Pseudomonas aminotransferase involved in caprolactam metabolism

Palacio, Cyntia M.; Rozeboom, Henriëtte J.; Lanfranchi, Elisa; Meng, Qinglong; Otzen, Marleen; Janssen, Dick B.

Published in:
The FEBS Journal

DOI:
10.1111/febs.14950

The FEBS Journal

FEBS PRESS science publishing by scientists

Biochemical properties of a *Pseudomonas* aminotransferase involved in caprolactam metabolism

Cyntia M. Palacio, Henriëtte J. Rozeboom, Elisa Lanfranchi, Qinglong Meng, Marleen Otzen and Dick B. Janssen

Biotransformation and Biocatalysis, Groningen Biomolecular Sciences and Biotechnology Institute (GBB), University of Groningen, The Netherlands

Keywords
6-aminohexanoic acid; aminotransferase; caprolactam; deamination; pyridoxal phosphate

Correspondence
D. B. Janssen, Biochemical Laboratory, Groningen Biomolecular Sciences and Biotechnology Institute, University of Groningen, Nijenborgh 4, Groningen 9747 AG, The Netherlands
Tel: +31 50 3634008
E-mail: d.b.janssen@rug.nl

(Received 16 October 2018, revised 29 April 2019, accepted 1 June 2019)

doi:10.1111/febs.14950

The biodegradation of the nylon-6 precursor caprolactam by a strain of *Pseudomonas jessenii* proceeds via ATP-dependent hydrolytic ring opening to 6-aminohexanoate. This non-natural ω-amino acid is converted to 6-oxohexanoic acid by an aminotransferase (*Pj*AT) belonging to the fold type I pyridoxal 5′-phosphate (PLP) enzymes. To understand the structural basis of 6-aminohexanoatate conversion, we solved different crystal structures and determined the substrate scope with a range of aliphatic and aromatic amines. Comparison with the homologous aminotransferases from *Chromobacterium violaceum* (*Cv*AT) and *Vibrio fluvialis* (*Vf*AT) showed that the *Pj*AT enzyme has the lowest K_M values (highest affinity) and highest specificity constant (k_{cat}/K_M) with the caprolactam degradation intermediates 6-aminohexanoate and 6-oxohexanoic acid, in accordance with its proposed *in vivo* function. Five distinct three-dimensional structures of *Pj*AT were solved by protein crystallography. The structure of the aldimine intermediate formed from 6-aminohexanoate and the PLP cofactor revealed the presence of a narrow hydrophobic substrate-binding tunnel leading to the cofactor and covered by a flexible arginine, which explains the high activity and selectivity of the *Pj*AT with 6-aminohexanoate. The results suggest that the degradation pathway for caprolactam has recruited an aminotransferase that is well adapted to 6-aminohexanoate degradation.

Database
The atomic coordinates and structure factors *P. jessenii* 6-aminohexanoate aminotransferase have been deposited in the PDB as entries 6G4B (E•succinate complex), 6G4C (E•phosphate complex), 6G4D (E•PLP complex), 6G4E (E•PLP-6-aminohexanoate intermediate), and 6G4F (E•PMP complex).

Introduction

Caprolactam is a bulk chemical mostly used for the industrial production of the polyamide nylon 6 [1]. This synthetic polymer has found widespread application in various industrial and household products, such as packaging materials, fibers and fabrics, utensils, and mechanical parts. In the nylon 6 manufacturing process, caprolactam undergoes a ring opening polymerization reaction at 240–270 °C in the presence of water. After the polymerization process, several undesired side products remain, including the unreacted lactam and 6-aminohexanoate monomers, oligomers, and cyclic dimers [2]. Caprolactam and its side products should be removed before waste or wastewater is discharged into the environment, since

Abbreviations
(*S*)-MBA, α-methylbenzylamine; 6-AHA, 6-aminohexanoic acid; AlaDH, alanine dehydrogenase; AT, aminotransferase; NAD, nicotinamide adenine dinucleotide; PLP, pyridoxal 5′-phosphate; PMP, pyridoxamine 5′-phosphate.

release into natural water streams will threaten environmental quality and public health. To understand the environmental fate of nylon-related compounds and their biodegradation, several studies have been carried out aimed at isolating microorganisms that metabolize caprolactam and 6-aminohexanoate (cyclic) oligomers [3–6]. Some of these strains contain plasmids that harbor genes involved in caprolactam utilization, including genes encoding 6-aminohexanoate dimer hydrolase and 6-aminohexanoato cyclic dimer hydrolase, which are responsible for hydrolysis of amide bonds [5–7]. Although a complete degradation pathway is also suggested in the MetaCyc database (see http://www.ebi.ac.uk/msd-srv/prot_int/pistart.html) [8], most enzymes of the caprolactam catabolic route remained unidentified until two rather different aminotransferases (AT) that may catalyze 6-aminohexanoate deamination were recently discovered [9,10]. Our lab described the caprolactam-utilizing bacterium *Pseudomonas jessenii* strain OGJ3, which produces an ATP-dependent lactamase that converts caprolactam to 6-aminohexanoate. This intermediate is converted by an aminotransferase that transfers the amino group to pyruvate and produces 6-oxohexanoic acid, which can be metabolized by β-oxidation via formation of adipic acid [10] (Fig. 1).

Aminotransferases are pyridoxal 5′-phosphate (PLP)-dependent enzymes that catalyze the transfer of an amino group from a donor (e.g. an amino acid or amine) to an acceptor, which *in vivo* is most often pyruvate or 2-oxoglutarate [11,12]. After binding of the substrate, in the first half reaction its amino group is transferred to the PLP cofactor via formation of an imine (external aldimine) and proton shift, leading to a pyridoxamine (E•PMP) intermediate. Following the release of the deaminated product as a ketone or aldehyde, in the second half reaction the enzyme binds the ketoacid acceptor and the amino group of PMP is transferred to this acceptor, again via imine formation and proton shift. The aminated product is released by cleavage of the Schiff base linkage under regeneration of enzyme-bound PLP. Based on crystal structures, PLP-dependent enzymes have been divided into different fold types, subgroups, and classes, which to a certain extend correlates to reaction type or substrate scope [13–15].

Aminotransferases often belong to fold type I or fold type IV PLP enzymes [12–16]. Examples of well-

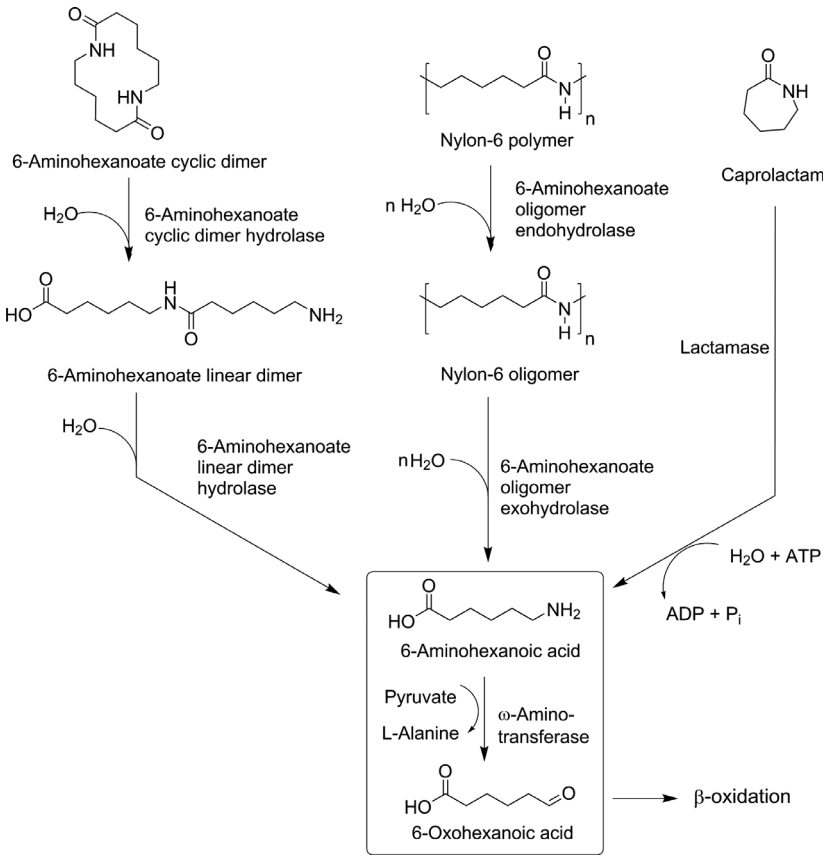

Fig. 1. Nylon 6, nylon 6-oligomer and caprolactam biodegradation. The catabolic pathways of 6-aminohexanoate (cyclic) dimers and oligomers [74,75] and the route of caprolactam degradation in *Pseudomonas jessenii* [10] converge to 6-aminohexanoate, which is deaminated in *P. jessenii* by the aminotransferase described here.

studied fold type I aminotransferases are L-aspartate ATs [17], branched L-amino acid ATs, β-amino acid ATs [18,19] and the ω-aminotransferases (ωATs) from *Vibrio fluvialis*, *Chromobacterium violaceum*, *Paracoccus denitrificans*, and *Ochrobactrum anthropi* [20–24]. Fold type IV enzymes include D-amino acid ATs and (*R*)-amine selective ωATs [11–14,25,26]. Aminotransferases have also been classified in subgroups or classes, mainly based on substrate structural features, leading to a classification that partially agrees with grouping in fold types [13,15]. The subgroup AT-I aminotransferase are active with α-amino acids and thus include the PLP fold type I aspartate ATs and branched L-amino acid ATs. The original AT-II subgroup [13], later also called class III ATs, includes ω-aminotransferases, that is, enzymes acting on non-α-amino acids [15]. The sequence suggests that the *P. jessenii* strain GO3 aminotransferase (*Pj*AT) of the caprolactam catabolic pathway is most similar to these class III ATs [10], of which structures and sequences have been compared in detail [15,23].

Aminotransferases offer a diversity of realized and potential biotechnological applications. They usually have a high catalytic activity and do not require an external redox cofactor recycling system if an organic amine is used as the donor [20,27–30]. Process conditions for amination reactions catalyzed by enzymes are milder than in case of chemocatalytic incorporation of amine groups, which can make the use of aminotransferases attractive from an environmental point of view [31]. Of particular interest is the production of chiral amines by asymmetric transformation of nonchiral keto-precursors. In such reactions, aminotransferases often show high regio-, enantio-, and chemoselectivity. Other attractive reactions are the terminal amination of aldehydes to produce amines, either in cascade conversions with free enzymes starting with ammonia and alcohol or by employing reactions with whole cells [32,33]. Recent work indicates that aminotransferases can be important for constructing artificial biosynthetic pathways, even leading to the biosynthesis of non-natural amines such as 6-aminohexanoate (6-AHA), the precursor of caprolactam [34]. Aminohexanoic acid is also used as an antifibrinolytic drug in surgery. It can prevent excessive blood loss by inhibiting tissue plasminogen activation [35].

To discover an aminotransferase involved in caprolactam metabolism and examine its potential use in various enzymatic transformations of biotechnological interest, we investigated the caprolactam degradation pathway of *P. jessenii* GO3, using a proteomic and genomic approach [10]. The aminotransferase (*Pj*AT) present in this strain acts in a catabolic pathway that involves compounds that are only known from chemical synthesis. The enzyme is examined here addressing the question if the enzyme is evolved to deaminate 6-aminohexanoic acid, a synthetic amino acid. The substrate range is determined and compared to that of related enzymes. We solved several crystal structures to explain the activity toward the biologically unknown substrate 6-AHA. We also examined the activity in the amination of 6-oxohexanoic acid and interpret the selectivity using 3D structures.

Results

Catalytic properties of *P. jessenii* 6-aminohexanoate aminotransferase

To overproduce the recently discovered *P. jessenii* aminotransferase involved in bacterial caprolactam degradation [10], we used a pET-based expression vector and *Escherichia coli* strain Top10. After overnight growth under inducing conditions, a high-level expression of soluble enzyme was reached. Preparation of cell lysate by sonication, centrifugation, and enzyme isolation by His-tag Ni-affinity chromatography yielded 34 mg of purified protein per 1 L of culture. This material was used for activity profiling and crystallography. The dimeric enzyme (49.64 kDa subunits) showed activity toward 6-aminohexanoate (6-AHA) and 6-oxohexanoic acid, the aminated and deaminated intermediates of the caprolactam and 6-aminohexanoate oligomer degradation pathways (Fig. 1). With 2 mM 6-aminohexanoate and pyruvate as amino donor, an activity of 0.9 $U \cdot mg^{-1}$ was found for the purified enzyme, corresponding to a k_{obs} of 0.3 s^{-1} (per subunit).

Compounds such as amino acids, aliphatic amines, and aromatic amine compounds are of interest for the production of various pharmaceuticals, paintings, and crop protectants [36,37]. Therefore, specific activities of *Pj*AT were measured using over 40 different amine substrates, including aromatic compounds, linear aliphatic compounds, and amino acids (Table 1). This activity screening was performed with spectrophotometric coupled-enzyme assays in which aminotransferase-mediated formation of L-alanine from pyruvate and 6-aminohexanoate was coupled to alanine dehydrogenase-mediated production of NADH. Data were compared to values measured with the aminotransferases from *V. fluvialis* (*Vf*AT, 42% sequence identity) and *C. violaceum* (*Cv*AT, 40% sequence identity).

The results (Table 1) showed that the *Pj*AT enzyme, as well as *Cv*AT and *Vf*AT, had high activities with aromatic compounds carrying the amine functionality

Table 1. Activities of *Pj*AT, *Cv*AT, and *Vf*AT.[a]

Name	Structure	Sp. act. (%)		
		*Pj*AT	*Cv*AT	*Vf*AT
(*S*)-α-Methylbenzylamine		100 (0.9)[b]	100 (1.6)[b]	100 (1.0)[b]
(*R*)-α-Methylbenzylamine		17	–[c]	–
6-Aminohexanoic acid (6-AHA)	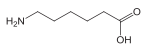	100	180	35
5-Aminopentanoic acid	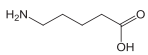	95	93	4
4-Aminobutanoic acid	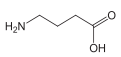	129	174	70
1-Aminoheptane	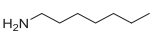	68	–	–
1-Aminohexane	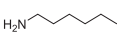	52	–	–
1-Aminopentane	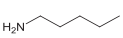	63	209	91
1-Aminobutane	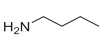	21	–	–
1-Propylamine		10	–	–
Benzylamine		208	406	208
2-Phenylethylamine	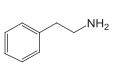	28	201	106
3-Phenylpropylamine	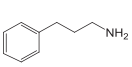	25	77	60
4-Phenylbutylamine	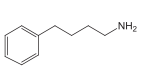	99	145	28
3-Fluorobenzylamine	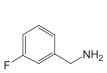	75.5	82.3	53.6
4-Fluorobenzylamine	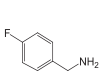	67.2	94.8	78.7

Table 1. (Continued).

Name	Structure	Sp. act. (%)		
		*Pj*AT	*Cv*AT	*Vf*AT
L-Serine		3.1	10.7	3.8
L-Leucine		< 1	4.7	18.6

[a]Reaction conditions: 15 mM of substrate, 0.2 mM pyruvate, 0.05 mM PLP, 5 U·mL^{-1} alanine dehydrogenase, 2 mM NAD, and 0.015 mg·mL^{-1} *Cv*AT, *Vf*AT or *Pj*AT, 30 °C, in 100 mM potassium phosphate, pH 8. Substrates for which no or very low activity was detected with all three enzymes include 2-(2-butoxyethoxy)ethanamine, 2-aminooctanoic acid, 1-butoxy-2-propanamine, (*S*)-3-amino-3-phenylpropanoic acid ethyl ester, (*S*)-3-amino-3-(p-hydroxyphenyl)propionic acid, L-serine, L-tyrosine, L-phenylalanine, L-ornithine, L-valine, L-aspartate, L-glutamate, L-tryptophan, L-alanine, β-(*R*)-phenylalanine, and β-(*R*)-tyrosine. *Pj*AT also showed no activity with L- and D-lysine, D-phenylalanine, D-ornithine, L- and D-glutamic acid, ethylamine, 1,3-diaminopropane, 1,4-diaminobutane, spermidine. [b]Activities are expressed as % of the activity found with (*S*)-α-methylbenzylamine. Values in parenthesis represent specific activities with (*S*)-α-methylbenzylamine (U·mg^{-1}). [c]Not determined.

on short aliphatic side groups, for example, α-methylbenzylamine ((*S*)-MBA) and benzylamine. For the latter two enzymes, this is in agreement with Kaulmann *et al.* [22] and Shin and Kim [38,39] who also observed that activities of *Cv*AT and *Vf*AT with benzylamines were higher than with aliphatic amines. Nevertheless, several aliphatic amines and the ω-amino acids, 4-aminobutanoic acid and 5-aminopentanoic acid, and the obvious 'natural' substrate 6-AHA also gave good activities, especially with *Pj*AT and *Cv*AT. Glycine and most other α-amino acids tested were not converted. We found that also *Cv*AT had high activity with 6-AHA, higher than found earlier [22]. Primary alkylamines similar to 6-AHA but with the carboxylate group replaced by a methyl or alkylamines carrying a phenyl group (4-aminophenylbutane) were also well converted by all three enzymes (Table 1).

Some of the tested compounds were a poor substrate for all three ATs examined. Three β-amino acids were tested, but none was converted by any of the enzymes (Table 1). This clearly distinguishes these aminotransferases from the homologous PLP fold type I β-amino acid aminotransferases discovered in bacterial cultures enriched with β-Phe as growth substrate [18,19,40]. Likewise, no good conversion of proteinogenic amino acids was found, in case of *Cv*AT and *Vf*AT agreement with Kaulman *et al.* [22] and Shin and Kim [41].

To further examine the apparent activity differences, kinetic studies were performed with the aminated substrates that gave the best activities as well as with 6-oxohexanoate, the direct deamination product of 6-AHA in the caprolactam degradation pathway (Table 2). The results revealed that of the three enzymes *Pj*AT has the highest affinities for 6-AHA and 6-OHA, with apparent K_M values that were at least sevenfold lower for the amine substrate and 33-fold lower in case of the aldehyde when compared to values for *Cv*AT and *Vf*AT. The k_{cat} values, on the other hand, were highest for *Cv*AT, but the physiologically most relevant k_{cat}/K_M value was best for *Pj*AT, in accordance with its function in caprolactam degradation. Interestingly, *Pj*AT had a lower apparent K_M with 6-OHA than with the amine donor 6-AHA, indicating that the enzyme might be used for aldehyde amination, a reaction of importance for caprolactam production by metabolically engineered *E. coli* [34]. At high substrate concentrations, however, substrate inhibition was observed with all three enzymes when using the aldehyde as an amine acceptor.

The results with other substrates confirmed that aryl-substituted alkylamines were well accepted by the three ω-aminotransferases (Table 2). With all amino compounds the highest k_{cat} values were observed with *Cv*AT, which was also found by Kaulmann *et al.* [22] when comparing *Cv*AT and *Vf*AT. Regarding affinities, it appeared that *Pj*AT, which displayed the highest affinity for 6-AHA, showed the poorest affinity in case of the aromatic substrates. This gave a preference for 6-AHA, expressed as ratio of k_{cat}/K_m values, which was 2- and 25-fold better for *Pj*AT compared to *Cv*AT and *Vf*AT, respectively.

The high substrate affinity of *Pj*AT was not only found with 6-AHA; also the shorter ω-amino acids 5-aminopentanoic acid and 4-aminobutanoic acid gave K_M values that were at least sixfold better in case of *Pj*AT. The carboxylate group of the ω-amino acids

Table 2. Steady-state kinetic parameters of the aminotransferases for linear aliphatic and aromatic substrates.[a]

Substrate	Enzyme	k_{cat} (s^{-1})[b]	K_M (mM)	K_I (mM)	k_{cat}/K_M ($mM^{-1}·s^{-1}$)
Caprolactam metabolism intermediates					
6-Aminohexanoate	*Pj*AT	0.3 ± 0.1	1.54 ± 0.1		0.2
	*Cv*AT	0.95 ± 0.02	10.6 ± 0.4		0.09
	*Vf*AT	0.58 ± 0.01	71 ± 2		0.008
6-Oxohexanoate[c]	*Pj*AT	5.4 ± 0.1	0.06 ± 0.01	12.6 ± 0.6	89
	*Cv*AT	11 ± 2	2.8 ± 0.9	3.3 ± 0.9	3.8
	*Vf*AT	1.8 ± 0.1	2 ± 0.2	11 ± 1	0.9
Linear aminated substrates					
5-Aminopentanoic acid	*Pj*AT	0.21 ± 0.01	0.9 ± 0.1		0.2
	*Cv*AT	0.35 ± 0.01	9.8 ± 0.4		0.04
	*Vf*AT	0.02 ± 0.01	8.2 ± 1.3		0.003
4-Aminobutanoic acid	*Pj*AT	0.26 ± 0.01	2.1 ± 0.1		0.1
	*Cv*AT	0.55 ± 0.01	2.3 ± 0.1		0.2
	*Vf*AT	0.3 ± 0.1	8.9 ± 0.4		0.03
1-Aminopentane	*Pj*AT	0.18 ± 0.01	8.5 ± 0.5		0.02
	*Cv*AT	1.1 ± 0.1	5.7 ± 0.5	117 ± 27	0.2
	*Vf*AT	0.6 ± 0.1	7.2 ± 0.7	64 ± 13	0.08
Aromatic aminated substrates					
Benzylamine	*Pj*AT	0.75 ± 0.04	1.8 ± 0.2	> 30	0.4
	*Cv*AT	≥ 1.6 ± 0.1[d]	≥ 1.0 ± 0.1[d]	18 ± 2[d]	1.6
	*Vf*AT	0.74 ± 0.02	0.61 ± 0.04	> 200	1.2
(S)-α-Methylbenzylamine	*Pj*AT	1.1 ± 0.1	2.1 ± 0.2	22 ± 2	0.5
	*Cv*AT	2.3 ± 0.1	1.3 ± 0.1	59 ± 7	1.7
	*Vf*AT	1.6 ± 0.1	1.1 ± 0.1	151 ± 38	1.5
2-Phenylethylamine	*Pj*AT	0.75 ± 0.04	81 ± 6		0.009
	*Cv*AT	0.72 ± 0.01	5 ± 0.1		0.2
	*Vf*AT	0.3 ± 0.1	3.6 ± 0.1		0.08
3-Phenylpropylamine	*Pj*AT	0.13 ± 0.01	2.4 ± 0.2	44 ± 6	0.05
	*Cv*AT	0.38 ± 0.01	1.7 ± 0.1	46 ± 4	0.2
	*Vf*AT	0.21 ± 0.01	0.77 ± 0.04		0.3
4-Phenylbutylamine	*Pj*AT	0.3 ± 0.1	1.5 ± 0.1	> 200	0.2
	*Cv*AT	0.43 ± 0.01	0.56 ± 0.04	> 100	0.8
	*Vf*AT	0.1 ± 0.01	0.71 ± 0.05		0.1

[a]Reactions with amine donors were carried out in triplicate with varying substrate concentrations (0.1–90 mM), 0.2 mM pyruvate, 0.05 mM PLP, 5 $U·mL^{-1}$ alanine dehydrogenase, and 0.015 $mg·mL^{-1}$ *Cv*AT, *Vf*AT, or *Pj*AT at 30 °C in 100 mM potassium phosphate, pH 8. [b]Values for k_{cat} are per subunit. [c]Substrate amination reactions were carried out in triplicate with 0.08–32 mM 6-oxohexanoate, 0.05 mM PLP, 0.1 mM NADH, 5 mM L-alanine, 5 mM ammonium bicarbonate, 8 $U·mL^{-1}$ *Bc*AlaDH, and 100 mM potassium phosphate buffer, pH 8, at 30 °C. [d]Only lower limits for k_{cat} and K_M were obtained due to complex substrate inhibition.

seems to favor *Pj*AT, since the higher affinity of this enzyme for ω-amino acids was not observed with other amines, such as 1-aminopentane and 2-phenylethylamine.

At high substrate concentration, substrate inhibition was observed with most of the aromatic compounds tested, with the exception of 2-phenylethylamine. This type of inhibition is in line with previous reports demonstrating that aminotransferases are inhibited by high concentrations of an aromatic substrate [38]. It is likely due to binding of the amine substrate to the pyridoxamine intermediate rather that binding of the oxo-substrate that accepts the amine group.

Summarizing, the kinetic properties indicate that *Pj*AT is a more suitable catalyst for 6-AHA deamination than *Cv*AT or *Vf*AT in case of low substrate concentrations. This raises the question if the substrate's carboxylate group located five carbons away from the reacting amine is involved in binding to the enzyme and in any evolutionary adaptation of *Pj*AT to 6-aminohexanoate conversion.

Crystal structures

The structure of *Pj*AT was determined by protein crystallography using molecular replacement and refinement against 1.80 Å resolution diffraction data to an *R*-factor of 0.141 (R_{free} = 0.166) with good stereochemistry (Table S1, Fig. 2). The protein is composed of two subunits forming a tight homodimer with an interface score

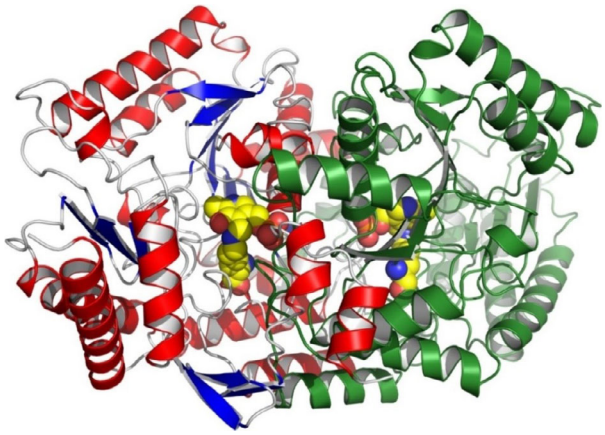

Fig. 2. Crystal structure of *Pseudomonas jessenii* aminotransferase. One subunit is colored in red/blue/gray and the other in green. The external aldimines of PLP bound to 6-aminohexanoate in both subunits are shown as yellow spheres. Residues from both subunits contribute to each active site.

calculated by PISA of 0.92 (http://www.ebi.ac.uk/msd-srv/prot_int/pistart.html). The dimeric *Pj*AT molecule has dimensions of 100 × 60 × 55 Å. The *Pj*AT structure is very similar to the structures of other PLP fold type I enzymes belonging to the ω-aminotransferases, with DALI *Z*-scores over 20, rmsd values ~ 0.8–1.2 Å and sequence identities of 40–63%. These include the recently described ω-aminotransferase from *O. anthropi* (5GHF); the putative aminotransferases from *Mesorhizobium loti* (3GJU, JCSG) and *Silicibacter* sp. TM1040 (3FCR, JCSG); the aminotransferase from *Silicibacter pomeroyi* (3HMU); the ω-aminotransferase from *P. denitrificans* (4GRX), and the aminotransferases included in the activity comparison above *Cv*AT ([4A6R] and *Vf*AT [3NUI]) (Fig. 3). Only 32% identity is observed with a *Pseudomonas aeruginosa* ω-aminotransferase (4B9B [42]) and a *Pseudomonas putida* ω-aminotransferase (3A8U, unpublished).

All these PLP fold type I aminotransferases group into Clade 6c of the class II/III ATs, most of which are dimeric ω-ATs with subunits consisting of two domains [23]. The smaller domain of *Pj*AT comprises residues 1–66 and 346–456. The large domain comprises residues 67–345 and contains most of the conserved residues, including residues that form the cofactor binding site.

The PLP-binding pockets of *Pj*AT are located at the dimeric interfaces and contain residues from both subunits. In the succinate and ammonium phosphate-grown crystals, a succinate or a phosphate ion, respectively, occupies the position of the phosphate moiety of the PLP in the homologous structures. The phosphates are hydrogen bonded to the backbone amides of Gly118 and Ser119, the backbone amide and side chain of Thr324', and five water molecules (Fig. 4A). The succinate molecule has the same interactions, including hydrogen bonds to the side chains of Ser286 and Lys287, to a water molecule and to a glycerol molecule (Fig. 4B). This glycerol molecule has hydrogen bonds to the carbonyl atoms of Asn116, Pro295 and to the carbonyl and side chain oxygens of Ser286. The glycerol occupies a small pocket shaped by Asn116, Ser292, Pro295, and Gly325'. In *Cv*AT and *Silicibacter* AT, this pocket is occupied by a side chain of a Tyr, while it also exists in *Vf*AT.

The PLP-binding pockets are well conserved between PLP fold type I class II or class III ATs [43]. In the *Pj*AT-PLP structure there is continuous electron density from the side chain of Lys287 to the cofactor, revealing the internal aldimine adduct of PLP (Fig. 5A). The pyridine ring is sandwiched between the perpendicular ring of Tyr151 and the isopropyl group of Val260. The nitrogen of the ring has interaction with the side chain of the conserved Asp258. Additional density was observed close to the PLP. This was modeled as a glycerol and interacts with the ε-amino group of the catalytic Lys287, and side chains of Trp58, Tyr151, Ala230, and Arg417. Its position is different from the glycerol in the succinate experiment, being at the other side of Thr324' at ~ 8 Å distance. The latter pocket is filled with water molecules in the *Pj*AT-PLP structure.

Electron density maps of the *Pj*AT-PLP crystal soaked with 6-AHA showed discontinuous residual density in subunit A between the ε-amino group of Lys287 and PLP, showing that the Schiff base bond is not present. Instead, additional density extending from the PLP carbonyl carbon was modeled as the 6-AHA external aldimine adduct (Fig. 5B). In subunit B the unreacted internal aldimine was observed. The

Fig. 3. Structure-based sequence alignment of eight PLP fold type I class III aminotransferases. Displayed are the sequences of *Pj*AT from *Pseudomonas jessenii, Oa*AT from *Ochrobactrum anthropi* (5GHF, [24]), a putative AT from *Mesorhizobium loti* maff303099 (*Ml*AT, 3GJU, JCSG), ω-AT from *Paracoccus denitrificans* (*Pd*AT, 4GRX, [23]), *Vf*AT from *Vibrio fluvialis* (4E3Q, [53]), AT from *Silicibacter pomeroyi* (*Sp*AT, 3HMU, NYSGXRC), a putative AT from *Silicibacter* sp. TM1040 (*Si*AT, 3FCR, JCSG), and *Cv*AT from *Chromobacterium violaceum* (4A6R, 4A6T, 4BA5 [42,44,45]). The sequences have more than 40% identity. The secondary structure elements above the sequence alignment are obtained from the crystal structure of *Pj*AT. Identical residues have a red background color and similar residues have a red color. Residues with a purple color are the catalytic lysine and with a green color line the active site, the cyan asterisks below the sequencMes indicate the position of the gateway Arg and Glu residues which are missing in the displayed sequences. The figure was created with ESPRIPT [72].

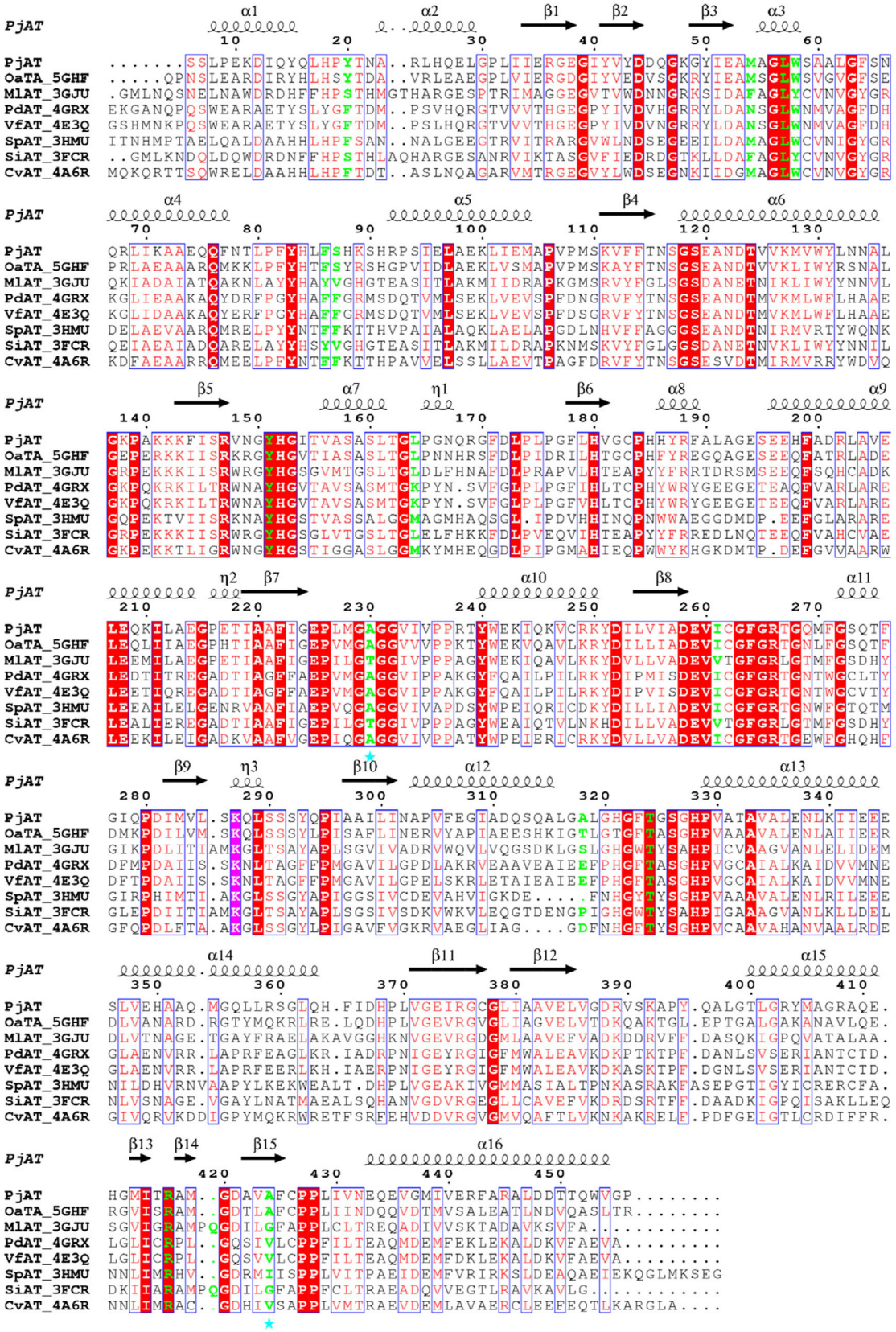
PjAT
α1 α2 β1 β2 β3 α3
10 20 30 40 50 60
PjAT .....SSLPEKDIQYQLHPYTNA..RLHQELGPLIIERGEGIYVYDDQGKGYIEAMAGLWSAALGFSN
OaTA_5GHF .....QPNSLEARDIRYHLHSYTDA..VRLEAEGPLVIERGDGIYVEDVSGKRYIEAMSGLWSVGVGFSE
MlAT_3GJU .GMLNQSNELNAWDRDHFFHPSTHMGTHARGESPTRIMAGGEGVTVWDNNGRKSIDAFAGLYCVNVGYGR
PdAT_4GRX EKGANQPQSWEARAETYSLYGFTDM..PSVHQRGTVVVTHGEGPYIVDVHGRRYLDANSGLWNMVAGFDH
VfAT_4E3Q GSHMNKPQSWEARAETYSLYGFTDM..PSLHQRGTVVVTHGEGPYIVDVNGRRYLDANSGLWNMVAGFDH
SpAT_3HMU ITNHMPTAELQALDAAHHLHPFSAN..NALGEEGTRVITRARGVWLNDSEGEEILDAMAGLWCVNLGYGR
SiAT_3FCR ..GMLKNDQLDQWDRDNFFHPSTHLAQHARGESANRVIKTASGVFIEDRDGTKLLDAFAGLYCVNVGYGR
CvAT_4A6R MQKQRTTSQWRELDAAHHLHPFTDT..ASLNQAGARVMTRGEGVYLWDSEGNKIIDGMAGLWCVNVGYGR
α4 α5 β4 α6
70 80 90 100 110 120 130
PjAT QRLIKAAEQQFNTLPFYHLFSHKSHRPSIELAEKLIEMAPVPMSKVFFTNSGSEANDTVVKMVWYLNNAL
OaTA_5GHF PRLAEAAARQMKKLPFYHTFSYRSHGPVIDLAEKLVSMAPVPMSKAYFTNSGSEANDTVVKLIWYRSNAL
MlAT_3GJU QKIADAIATQAKNLAYYHAYVGHGTEASITLAKMIIDRAPKGMSRVYFGLSGSDANETNIKLIWYYNNVL
PdAT_4GRX KGLIEAAKAQYDRFPGYHAFFGRMSDQTVMLSEKLVEVSPFDNGRVFYTNSGSEANDTMVKMLWFLHAAE
VfAT_4E3Q KGLIDAAKAQYERFPGYHAFFGRMSDQTVMLSEKLVEVSPFDSGRVFYTNSGSEANDTMVKMLWFLHAAE
SpAT_3HMU DELAEVAARQMRELPYYNTFFKTTHVPAIALAQKLAELAPGDLNHVFFAGGGSEANDTNIRMVRTYWQNK
SiAT_3FCR QEIAEAIADQARELAYYHSYVGHGTEASITLAKMILDRAPKNMSKVYFGLGGSDANETNVKLIWYYNNIL
CvAT_4A6R KDFAEAARRQMEELPFYNTFFKTTHPAVVELSSLLAEVTPAGFDRVFYTNSGSESVDTMIRMVRRYWDVQ
β5 α7 η1 β6 α8 α9
140 150 160 170 180 190 200
PjAT GKPAKKKFISRVNGYHGITVASASLTGLPGNQRGFDLPLPGFLHVGCPHHYRFALAGESEEHFADRLAVE
OaTA_5GHF GEPERKKIISRKRGYHGVTIASASLTGLPNNHRSFDLPIDRILHTGCPHFYREGQAGESEEQFATRLADE
MlAT_3GJU GRPEKKKIISRWRGYHGSGVMTGSLTGLDLFHNAFDLPRAPVLHTEAPYYFRRTDRSMSEEQFSQHCADK
PdAT_4GRX GKPQKRKILTRWNAYHGVTAVSASMTGKPYN.SVFGLPLPGFIHLTCPHYWRYGEEGETEAQFTVARLARE
VfAT_4E3Q GKPQKRKILTRWNAYHGVTAVSASMTGKPYN.SVFGLPLPGFVHLTCPHYWRYGEEGETEEQFVARLARE
SpAT_3HMU GQPEKTVIISRKNAYHGSTVASSALGGMAGMHAQSGL.IPDVHHINQPNWWAEGGDMDP.EEFGLARARE
SiAT_3FCR GRPEKKKIISRWRGYHGSGLVTGSLTGLELFHKKFDLPVEQVIHTEAPYYFRREDLNQTEEQFVAHCVAE
CvAT_4A6R GKPEKKTLIGRWNGYHGSTIGGASLGGMKYMHEQGDLPIPGMAHIEQPWWYKHGKDMTP.DEFGVVAARW
η2 β7 α10 β8 α11
210 220 230 240 250 260 270
PjAT LEQKILAEGPETIAAFIGEPLMGAGGVIVPPRTYWEKIQKVCRKYDILVIADEVICGFGRTGQMFGSQTF
OaTA_5GHF LEQLIIAEGPHTIAAFIGEPVMGAGGVVVPPKTYWEKVQAVLKRYDILLIADEVICGFGRTGNLFGCSQTF
MlAT_3GJU LEEMILAEGPETIAAFIGEPILGTGGIVPPPAGYWEKIQAVLKKYDVLLVADEVVTGFGRLGTMFGSDHY
PdAT_4GRX LEDTITREGADTIAGFFAEPVMGAGGVIPPAKGYFQAILPILRKYDIPMISDEVICGFGRTGNTWGCLTY
VfAT_4E3Q LEETIQREGADTIAGFFAEPVMGAGGVIPPAKGYFQAILPILRKYDIPVISDEVICGFGRTGNTWGCVTY
SpAT_3HMU LEEAILELGENRVAAFIAEPVQGAGGVIVAPDSYWPEIQRICDKYDILLIADEVICGFGRTGNWFGTQTM
SiAT_3FCR LEALIERGADTIAAFIGEPILGTGGIVPPPAGYWEAIQTVLNKHDILLVADEVVTGFGRLGTMFGSDHY
CvAT_4A6R LEEKILEIGADKVAAFVGEPIQGAGGVIVPPATYWPEIERICRKYDVLLVADEVICGFGRTGEWFGHQHF
β9 η3 β10 α12 α13
280 290 300 310 320 330 340
PjAT GIQPDIMVLSKQLSSSYQPIAAILINAPVFEGIADQSQALGALGHGFTGSGHPVATAVALENLKIIEEE
OaTA_5GHF DMKPDILVMSKQLSSSYLPISAFLINERVYAPIAEESHKIGTLGTGFTASGHPVAAAVALENLAIIEER
MlAT_3GJU GIKPDLITIAMKGLTSAYAPLSGVIVADRVWQVLVQGSDKLGSLGHGWTYSAHPICVAAGVANLELIDEM
PdAT_4GRX DFMPDAIISSKNLTAGFFPMGAVILGPDLAKRVEAAVEAIEEFPHGFTASGHPVGCAIALKAIDVVMNE
VfAT_4E3Q DFTPDAIISSKNLTAGFFPMGAVILGPELSKRLETAIEAIEEFPHGFTASGHPVGCAIALKAIDVVMNE
SpAT_3HMU GIRPHIMTIAKGLSSGYAPIGGSIVCDEVAHVIGKDE.....FNHGYTYSGHPVAAAVALENLRILEEE
SiAT_3FCR GLEPDIITIAMKGLTSAYAPLSGSIVSDKVWKVLEQGTDENGPIGHGWTYSAHPIGAAAGVANLKLLDEL
CvAT_4A6R GFQPDLFTAAKGLSSGYLPIGAVFVGKRVAEGLIAG....GDFNHGFTYSGHPVCAAVAHANVAALRDE
α14 β11 β12 α15
350 360 370 380 390 400 410
PjAT SLVEHAAQ.MGQLLRSGLQH.FIDHPLVGEIRGCGLIAAVELVGDRVSKAPY.QALGTLGRYMAGRAQE.
OaTA_5GHF DLVANARD.RGTYMQKRLRE.LQDHPLVGEVRGVGLIAGVELVTDKQAKTGL.EPTGALGAKANAVLQE.
MlAT_3GJU DLVTNAGE.TGAYFRAELAKAVGGHKNVGEVRGDGMLAAVEFVADKDDRVFF.DASQKIGPQVATALAA.
PdAT_4GRX GLAENVRR.LAPRFEAGLKR.IADRPNIGEYRGIGFMWALEAVKDKPTKTPF.DANLSVSERIANTCTD.
VfAT_4E3Q GLAENVRR.LAPRFEERLKH.IAERPNIGEYRGIGFMWALEAVKDKASKTPF.DGNLSVSERIANTCTD.
SpAT_3HMU NILDHVRNVAAPYLKEKWEALT.DHPLVGEAKIVGMMASIALTPNKASRAKFASEPGTIGYICRERCFA.
SiAT_3FCR NLVSNAGE.VGAYLNATMAEALSQHANVGDVRGEGLLCAVEFVKDRDSRTFF.DAADKIGPQISAKLLEQ
CvAT_4A6R GIVQRVKDDIGPYMQKRWRETFSRFEHVDDVRGVGMVQAFTLVKNKAKRELF.PDFGEIGTLCRDIFFR.
β13 β14 β15 α16
420 430 440 450
PjAT HGMITRAM..GDAVAFCPPLIVNEQEVGMIVERFARALDDTTQWVGP.....
OaTA_5GHF RGVISRAM..GDTLAFCPPLIINDQQVDTMVSALEATLNDVQASLTR.....
MlAT_3GJU SGVIGRAMPQGDILGFAPPLCLTREQADIVVSKTADAVKSVFA.....
PdAT_4GRX LGLICRPL..GQSIVLCPPFILTEAQMDEMFEKLEKALDKVFAEVA.....
VfAT_4E3Q LGLICRPL..GQSVVLCPPFILTEAQMDEMFDKLEKALDKVFAEVA.....
SpAT_3HMU NNLIMRHV..GDRMISPPLVITPAEIDEMFVRIRKSLDEAQAEIEKQGLMKSEG
SiAT_3FCR DKIIARAMPQGDILGFAPPFCLTRAEADQVVEGTLRAVKAVLG.....
CvAT_4A6R NNLIMRAC..GDHIVSAPPLVMTRAEVDEMLAVAERCLEEFEQTLKARGLA....

structure of the 6-AHA–derived external aldimine revealed that the tunnel-like substrate-binding site is shaped by several mostly hydrophobic residues from both subunits. Tyr20, Met54, Leu57, Trp58, Tyr151, Leu164, Ile261, Ala230, Arg417, Met419, Phe86', Ser87', and Ala318' provide a rather nonpolar substrate-binding site. Upon binding of 6-AHA, Met419 obtains a double conformation with a new conformation pointing toward the substrate (Fig. 5B). The new position is possible by a switch of the side chain of Arg417, which is very mobile and adopts a different conformation in all five determined *Pj*AT structures. High flexibility of an arginine corresponding to *Pj*AT's Arg417 is observed in other ATs as well [23,42,44]. In the 6-AHA aldimine adduct of *Pj*AT, Arg417 forms a bidentate salt bridge with the carboxylate of 6-AHA through the N^{ε} and N^{η} of the Arg417 side chain (3.8 and 3.7 Å distance), and there is an additional hydrogen bond of one of the carboxylate oxygens with the indole nitrogen of Trp58 (3.7 Å). Other contacts between substrate and enzyme are mainly hydrophobic, through the sidechains of Tyr20, Leu57, Phe86', and Tyr151 (Fig. 5B). In electron density maps of the crystal soaking experiment with (*S*)-MBA, PMP was observed, but no density for (*S*)-MBA emerged in subunit A, showing that the first half reaction has been completed (Fig. 5C). In subunit B, the internal aldimine was observed similar to the complex found in subunit B in the 6-AHA binding study. The structures determined of *Pj*AT resemble most the structures of *Oa*AT with PMP bound (5GHF), of *Cv*AT with PLP bound (PDB 4A6T) and with gabaculine-PLP bound (*m*-carboxyphenyl pyridoxamine phosphate) (4BA5) [24,42,45].

The results provide no indication of a major conformational change upon substrate binding since (aside from the mobility of Arg417 and Met419) the structures of *Pj*AT with PLP, PMP, phosphate, succinate, and the external aldimine formed with 6-AHA were very similar, as also observed in the *P. aeruginosa* transaminase [42]. However, conformational changes upon binding of a phosphate or phosphate mimic of several loops involved in structuring the active site may be possible in ATs, like displayed in *Cv*AT [45,44]. Both *Cv*AT and *Vf*AT have phenylalanine side chains pointing toward the conserved arginine (Arg417 in *Pj*AT), and restricting space at the active site entrance (Fig. 6). A major conformational change associated with 6-AHA binding is not necessary in *Pj*AT since Ser87, opposite to Arg417 in the active site, leaves enough space for the repositioning of Arg417 to a position where it can form a salt bridge with the carboxylate group of 6-ACA.

Discussion

The recently identified *P. jessenii* ω-transaminase, involved in the degradation of caprolactam, was studied after expressing the enzyme in *E. coli* by measuring substrate selectivities and examining various crystal structures. The sequence and the structure indicate that the enzyme is a class III aminotransferase (or AT-II subgroup) of the fold type I superfamily of PLP enzymes. To examine if and why the enzyme shows exceptional activity with 6-AHA and 6-OHA, which are intermediates of the caprolactam degradation pathway, activities were measured with a range of substrates, and compared to those found with well-characterized ω-aminotransferases from *C. violaceum* and *V. fluvialis*. The results showed that at low concentrations 6-AHA and 6-OHA are better substrates for the new *Pj*AT as compared to these reference ω-ATs, suggesting that the enzyme has indeed evolved for efficient deamination of the 6-AHA intermediate formed by enzymatic ring opening of caprolactam. The specificity constant (k_{cat}/K_M)

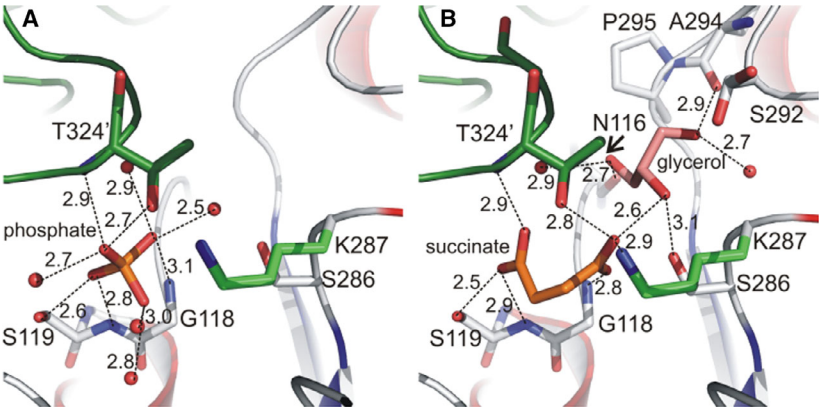

Fig. 4. Active site structure of *Pj*AT. (A) Binding of a phosphate ion (in orange) in ammonium phosphate-grown crystals. (B) Binding of a succinate molecule (in orange) in the phosphate-binding site. The glycerol molecule (in pink) occupies a small pocket. The residues forming the active site are displayed as sticks in cpk colors, Lys287 in green and Thr324' from the other subunit in dark green. Waters are depicted as red spheres. Hydrogen bonds are shown as dotted lines with indicated distances in Å. Ser292 shows a double conformation.

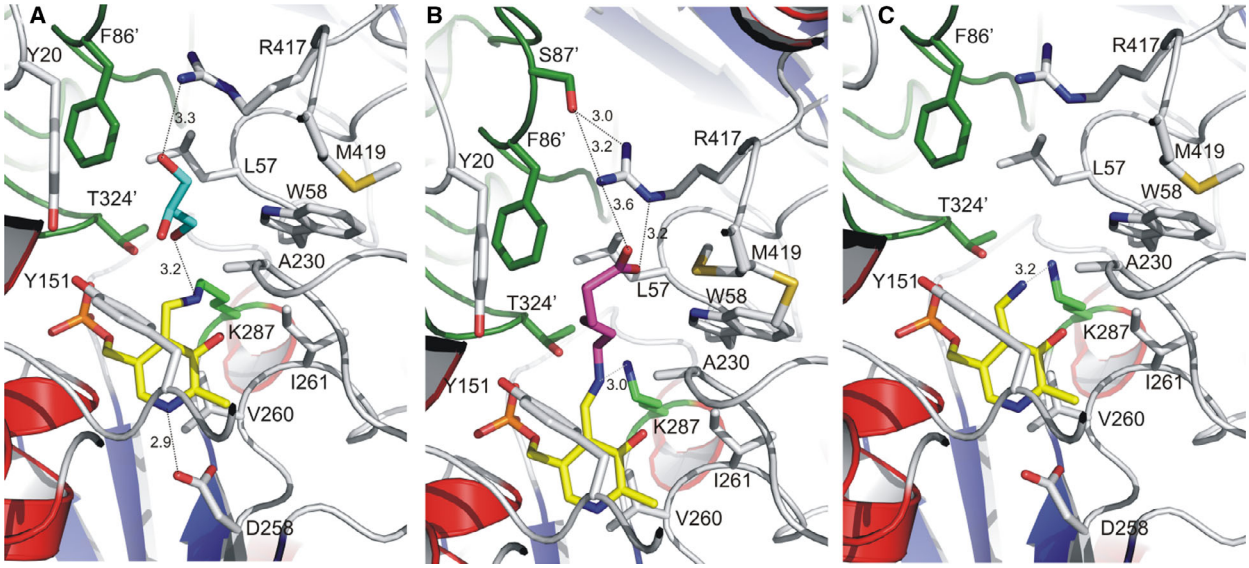

Fig. 5. Structures of the active site of *Pj*AT with PLP in different forms. (A) Internal aldimine with PLP (yellow) bound to the ε-nitrogen of Lys287 (light green) as a Schiff base. (B) Structure of the 6-AHA–PLP (yellow-magenta) external aldimine adduct, with Arg417 forming a bidentate salt bridge to the carboxylate of 6-AHA. Residue Met419 presents a double conformation. (C) PLP in the pyridoxamine (PMP) form after reaction with (*S*)-MBA. Residues forming the active site are displayed as sticks in cpk colors, Lys287 in green, Phe86′ and Ser87′ from the other subunit in dark green and the glycerol molecule in cyan. Black dotted lines with distances in Å indicate hydrogen bonds.

found with 6-AHA was 2–20-fold better for the *P. jessenni* enzyme, mainly due to the much higher K_M of *Vf*AT and *Cv*AT. The same is found for the aldehyde 6-OHA: the k_{cat}/K_M is at least 25-fold better in case of *Pj*AT than with the other ATs and the k_{cat}/K_M with 6-OHA is also at least 40-fold better than that with all the other tested amine substrates. *In vivo* levels of intermediates formed during caprolactam metabolism are unknown and may vary, but at high concentrations the aldehyde may be inhibitory for all three enzymes, as indicated by substrate inhibition. Substrate inhibition by the ketone or aldehyde acceptor observed in aminotransferases may be due to binding to the PLP form of the enzyme in competion with the amine donor. Similarly, substrate inhibition by the amine donor may be due to binding to the PMP form of the enzyme in competition with acceptor [38,39]. These effects make it difficult to assess the relevance of differences in kinetic constants for growth kinetics, but the structural studies provided further indications for a dedicated role for the *Pj*AT enzyme in 6-AHA metabolism. This role is in agreement with the upregulation of *Pj*AT found in proteomics experiments by Otzen *et al.* [10] when comparing cells growing on caprolactam with controls growing on glucose and ammonia.

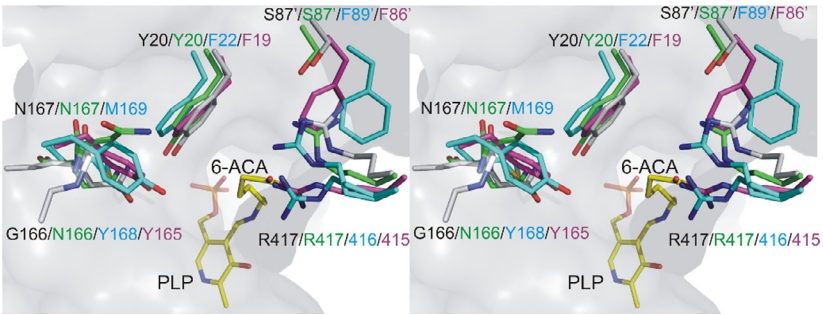

Fig. 6. Overlay of the active sites of PLP-bound forms of *Pj*AT, *Oa*AT, *Cv*AT, and *Vf*AT in stereo view. *Pj*AT in gray, with internal aldimine complex in yellow, *Oa*AT PMP bound form (PDB code 5GHF) in green, *Cv*AT PLP bound form (4AH3) in cyan (with R416 in double conformation), and *Vf*AT in the PMP bound form (4E3Q) in magenta. Only residues that differ between the three enzymes and the flexible arginine are shown.

Members of the class III ATs catalyze transfer of the amino group from an ω-amino acid, β-amino acid or from nonamino acid amines to an α-keto acid acceptor, producing an α-amino acid. Yet, these enzymes have little or no activity with α-amino acids as substrates, as found here with *Pj*AT, and thus apparently prevent the reaction of α-amino groups flanking an α-carboxylate functionality with the cofactor. Several of these ω-ATs, such as γ-aminobutyrate aminotransferase [46] and ornithine aminotransferase [47], use 2-oxoglutarate as an amine acceptor in the second half reaction and deploy a gateway system to prevent reactions at α-amino groups of amino acids [15]. This gateway consists of a juxtaposed pair of glutamate and arginine that forms a salt bridge during the first half reaction, thereby avoiding a stabilizing interaction of the arginine with the carboxylate of an α-amino acid. In the second half reaction, the gateway salt bridge is lost and the arginine can interact with the α-carboxylic group of the acceptor 2-oxoglutarate.

The Arg-Glu gateway pair is present at conserved positions in the sequence of class III ATs (Table S2), but the sequences (Fig. 3) and structure (Fig. 5) indicate that *Pj*AT and its close relatives (e.g., *Vf*AT, *Cv*AT, > 30% identity) do not employ such a gateway system. Sequence alignments (Fig. 3) derived from a structure-based phylogenetic tree (Fig. S1, Table S2) show that *Pj*AT contains two alanines at the Arg-Glu gateway positions. Accordingly, *Pj*AT has a preference for pyruvate over 2-oxoglutarate as an amine acceptor. Instead of the gateway arginine in the last β-strand (Arg412 in ornithine aminotransferase, PDB 1OAT/2CAN) *Pj*AT posesses an arginine (Arg417, which interacts with carboxylate of 6-AHA) on a stretch of sequence (a short β-strand in *Pj*AT) that is more outward and connects the preceding α-helix to the last β-strand. The external aldimine of *Pj*AT with pyruvate (alanine) bound can be modeled by superimposing *Arthrobacter* AT with Ala bound (PDB 5G2Q) on *Pj*AT with 6-ACA bound. The rotamer of Arg417 (Arg442 in 5G2Q) is altered so that it stabilizes the external aldimine by interacting with the carboxylate group of Ala. This movement of Arg417 can be regarded as a switch which moves the guanidine group of Arg417 from a position where it interacts with the carboxylate of 6-ACA in the first half reaction to a position where it interacts with the carboxylate of the alanine formed in the second half reaction. The hydrophobic side chain of Arg417 is sandwiched between Met54 and Met419 and the Nε of Trp58 could also help in stabilizing the alanine carboxylate. Furthermore, *Pj*AT can convert no α-amino acids, except for a very low activity with an α-amino acid with a very small side group such as serine. This can be due to the switching arginine occupying the tunnel the tunnel leading to the active site, which is also called the O-pocket because it is in the vicinity of the O3′ atom of PLP [15,48]. Arginine 417 could move in, to bind a carboxylate group, but this would leave insufficient space for larger α-amino acid side chains. A spacious pocket, like the P-pocket present in other class III ATs for binding bulky side chains, is also lacking. Thus, in comparison to Orn-AT, *Pj*AT has a different mechanism for rejecting α-amino acids and ketoglutarate as substrates. *Pj*AT is also different from the 6-AHA-deaminating aminotransferase proposed by Takehara *et al.* [9] to be involved in 6-AHA degradation by *Arthrobacter* sp. KI72. There is only low similarity (27% sequence identity), and the sequence of the *Arthrobacter* protein suggests it does have a gateway system, like 4-aminobutyrate aminotransferase.

In *Pj*AT, the flexible arginine Arg417 plays an important role in the first half reaction, when it interacts with the carboxylate of 6-ACA as shown by the crystal structure of the external aldimine. In ornithine δ-aminotransferase (Orn-AT, PDB 2CAN), the carboxylate of the bound substrate interacts with an arginine at a different position, that is, Arg180, which is called the switching arginine. An arginine at the corresponding position is missing in *Pj*AT. In Orn-AT, the (nonreacting) α-amino group interacts with the hydroxyl group of Tyr55 [47]. In lysine ε-aminotransferase (Lys-AT, PDB 2CJD) the carboxylate interacts with Arg170 (switch) and the amine with Asn328 [49], and the N328A mutant has negligible lysine ε-aminotransferase activity [50]. Interestingly, the sidechains Tyr55 of Orn-AT and Asn328 of Lys-AT are at similar positions in the active sites. In contrast, *Pj*AT has a Gly at that position in the structure and thus lacks the specific contacts (hydrogen bonds) necessary to stabilize the α-amine of L-lysine or L-ornithine, explaining our observation that these substrates are not accepted for ε- or δ-demination. Positioning of L-lysine in the active site for ε-deamination would introduce a positive charge close to the iminium of Arg417.

*Pj*AT also does not convert β-amino acids, in contrast to β-phenylalanine aminotransferases from *Variovorax paradoxus* (PDB 4AOA) and *Mesorhizobium* (PDB 2YKX [48]. Both of these enzymes can also accept α-amino acids. In these dual-substrate specificity enzymes, the carboxylate groups of β-amino acids are stabilized by Arg41/54 and a backbone amide of Gly299/313, and those of α-amino acids by Arg398/412. Arg417 in *Pj*AT is shifted only 1 residue from Arg398/412. However, *Pj*AT has no stabilization for β-amino acids, a carboxylate at that position in the

substrate would collide with the sidechain of Phe86, and due to the absence of a spacious P pocket the active site is too narrow for accomodating bulky side chains.

The well-studied mitochondrial Asp-AT belongs to the class I group of aminotransferases of the PLP fold-type I enzymes [15]. Although their sequences only have 9% sequence identity, the structures of *Pj*AT and Asp-AT are similar (RMSD of 3.5 Å on 280 aligned residues) (Fig. S2). However, *Pj*AT does not show the closure of the active site upon substrate binding that is well established for Asp-AT [51]. The mode of substrate binding is also quite different. Asp-AT has 2 arginines for stabilization of the substrates: Arg386 for the α-caboxylic group and Arg292 for the β-carboxylic group of the aspartate. Both are absent at the corresponding topological postions on strand/loop in *Pj*AT.

Comparison of the crystal structures of the related Class III enzymes *Pj*AT, *Cv*AT, and *Vf*AT and the recently solved structure of *O. anthropi* ω-aminotransferase (*Oa*AT) showed that both the overall structures and the active sites are well conserved. Subtle differences can be observed in the Gly166-Asn167 (*Pj*AT) loop which approaches the active site in *Pj*AT and *Oa*AT, whereas in the corresponding regions of *Cv*AT (Tyr168-Me169) and *Vf*AT (Tyr165-Asn166), the backbone structure is further outward (Fig. 6). The distance of the Tyr-OH to the flexible arginine is about 7 Å in *Vf*AT and *Cv*AT, while the shortest distance from Asn167 to the 6-AHA substrate in *Pj*AT is 6.5 Å. These distances are too long for any interaction. Another difference is the presence of Tyr20 in *Pj*AT and *Oa*AT, which is hydrogen bonded to the Asn in the Gly166-Asn167 loop. There is a Phe at this position in the other two ATs, making the subsite in *Pj*AT smaller and slightly more polar. Further comparison of the active sites suggest a cause of the better recognition of 6-AHA by *Pj*AT. In *Vf*AT, *Cv*AT, and other ω-aminotransferases a Phe is conserved at position 87, whereas a Ser is present in *Pj*AT and the more similar *Oa*AT. The smaller Ser facilitates an outward motion of Arg417 that leads to a salt bridge with the terminal carboxylate of 6-AHA, rather than a collision. In line with this finding, previous studies using *Vf*AT revealed that its substrate scope can be altered by mutagenesis of the active site. Cho *et al.* [52] demonstrated that the substitution of the conserved Trp57 and 147 with a Gly residue enabled *Vf*AT to accept longer aliphatic chain substrates, and Arg415 is replaced in several protein engineering studies [53–58]. The creation of space that allows outward movement of Arg417 by the Phe to Ser substitution at position 87 in *Pj*AT, which in turn makes space for the 6-ACA carboxylate, may be one of the adaptations of the enzyme to a role in caprolactam metabolism.

Substrate scope analyses and kinetic studies have shown a preference of the three aminotransferases examined here toward aromatic substrates. This is in line with previous studies using *Cv*AT and *Vf*AT [22,40]. Interestingly, *Pj*AT revealed lower catalytic efficiency toward the linear substrate 1-aminopentane in comparison to 4-aminobutanoic acid. The carboxylate group in the latter substrate will also be recognized by the flexible Arg417 [57], allowing better substrate binding. In contrast, *Vf*AT and *Cv*AT showed the best activity with 1-aminopentane in comparison with the other linear amines tested. As mentioned, in *Pj*AT, residue Ser87 replaces a phenylalanine in *Cv*AT and *Vf*AT, therefore, Arg417 is in a more polar environment and the combined effect may cause binding of the apolar 1-aminopentane to be unfavorable in *Pj*AT.

In conclusion, we showed that *Pj*AT has a nonpolar active site that is shaped mainly by aromatic side chains, such as Tyr and Phe. The high sequence similarity and the conserved secondary structure confirm the identity of the enzyme as an ω-transaminase. The high catalytic efficiency and the low K_M of *Pj*AT with 6-AHA and 6-OHA in combination with the residue configuration in the active site explain the role of *Pj*AT in the caprolactam/nylon 6 degradation pathway.

Materials and methods

Substrates and chemicals

Nicotinamide adenine dinucleotide (NAD) and alanine dehydrogenase from *Bacillus cereus* (*Bc*AlaDH) were purchased from Sigma-Aldrich (Zwijndrecht, the Netherlands). Pyridoxal phosphate (PLP) was purchased from Fisher Scientific (Landsmeer, the Netherlands). Potassium phosphate dibasic trihydrate and potassium phosphate monobasic were obtained from Merck (Schiphol-Rijk, the Netherlands). The substrates 6-aminohexanoato, 5-aminopentanoic acid, 1-aminopentane, 4-aminobutanoic acid, L-lysine, glycine, (*S*)-(–)-α-methylbenzylamine, benzylamine, 2-phenylethylamine, 4-phenylbutylamine, and 3-phenylpropylamine were purchased from Sigma-Aldrich. We synthesized 6-oxohexanoic acid as described by Bouet *et al.* [59].

Enzyme expression and purification

The isolation and characterization of *P. jessennii* strain GO3 was recently described by Otzen *et al.* [10]. Its 6-aminohexanoate aminotransferase was produced in *E. coli* strain Top10 using the *Pj*AT gene cloned in-frame

downstream of the hexahistidine tag sequence in expression vector pET20b(+). The coding sequence was obtained by PCR amplification of genomic DNA extracted from strain GO3. Derivatives of the expression vector pET28b(+) containing an in-frame fusion of the *C. violaceum* aminotransferase (*Cv*AT, NP_901695) or the *V. fluvialis* aminotransferase (*Vf*AT, AEA39183) were described by Palacio *et al.* [32]. The ω-aminotransferases *Pj*AT, *Cv*AT, and *Vf*AT were expressed in *E. coli* strain C41 and purified to homogeneity using His-tag metal affinity chromatography followed by a desalting step, as described earlier [32].

Activity assays

The activities of *Pj*AT, *Cv*AT, and *Vf*AT coupled with pyruvate amination were measured using an indirect assay by following alanine-dependent reduction of NAD^+ by alanine dehydrogenase at 340 nm ($\varepsilon_{NADH} = 6.22 \times 10^3$ M^{-1}·cm^{-1}) [60]. Excess alanine dehydrogenase from *B. cereus* (*Bc*AlaDH) was added to the reaction mixtures to ensure that the rate-limiting step is the transamination reaction. The pyruvate concentration was optimized to ensure high *Bc*AlaDH activities and a minimal lag phase. The reaction mixtures contained variable concentrations of substrate, 2 mM NAD^+, 0.05 mM PLP, 5 U·mL^{-1} *Bc*AlaDH, 0.015 mg·mL^{-1} aminotransferase, and 0.2 mM pyruvate in 100 mM potassium phosphate, pH 8. Assays were performed in flat-bottomed 96-well microtiter plates. The absorbance at 340 nm was monitored during 30 min at 30 °C using a microtiter plate reader (Synergy Mx Microplate Reader; BioTek Instrument, Winooski, VT, USA). The plates were prewarmed and reactions were started by addition of 150 μL of 0.4 mM pyruvate solution to 150 μL reaction mixture. All assays were done in triplicate. The initial rates of the reduction of NAD^+ observed with different substrate concentrations were used to determine the kinetic constants. Specific activities are expressed in units per mg of protein (μmole·min^{-1}·mg^{-1}).

Amination of 6-oxohexanoic acid was also measured using the coupled assay, that is, by following the pyruvate-dependent oxidation of NADH by alanine dehydrogenase. The reaction mixtures contained 100 mM potassium phosphate buffer (pH 8), 2 mM substrate, 0.1 mM NADH, 0.05 mM PLP, 8 U·mL^{-1} *Bc*AlaDH, 5 mM ammonium bicarbonate, 5 mM L-alanine and varying concentrations of substrate in a total volume of 300 μL. Reactions were initiated by the addition of L-alanine and carried out as described above.

Crystallization and X-ray data collection

The protein was concentrated to 10.5 mg·mL^{-1} in 25 mM HEPES buffer pH 7.5 using a Vivapsin Turbo 4 30K filter unit (Sartorius, Nieuwegein, the Netherlands). Initial vapor diffusion crystallization experiments were performed using a Mosquito crystallization robot (Molecular Dimensions Ltd, Newmarket, UK). Various commercially available crystallization screens were used, for example, JCSG+ and PACT (Qiagen Systems, Germantown, MD, USA) and Cryo (Emerald Biosystems, Bainbridge Island, WA, USA). *PjAT* crystals were obtained at room temperature from succinate and ammonium phosphate (both pH ~ 7.5) solutions. Optimization of the crystallization conditions yielded well-diffracting colorless crystals that grew within a few days when 1 μL protein solution (7.5 mg·mL^{-1}) was mixed with 1 μL reservoir solution containing 0.7–1.0 M ammonium phosphate or succinate, pH 7.3. Yellow PLP-containing protein crystals could be grown by first incubating *PjAT* with 0.1 mM fresh PLP for a few hours and using succinate as precipitant.

Before data collection, crystals were briefly soaked in a cryoprotectant solution consisting of 30% glycerol and 1.2 M succinate, pH 7.5, in 30% glycerol and 1.2 M ammonium phosphate, pH 7.5, or in 30% glycerol, 1.2 M succinate, and 0.1 mM PLP. The ligand complexes were obtained by soaking a PLP-containing crystal in succinate solution containing 0.4 M 6-AHA or (*S*)-(–)-α-methylbenzylamine ((*S*)-MBA) for 30 s and then briefly soaked in cryoprotectant including 6-AHA or (*S*)-MBA. X-ray diffraction data were collected with an in-house MarDTB Goniostat system using Cu-Kα radiation from a Bruker MicrostarH rotating-anode generator equipped with HeliosMX mirrors at 100 K. Intensity data were processed using XDS [61] and the CCP4 package [62]. The space group was $P4_3$, with unit cell dimensions of $a = b = 98.4$ Å and $c = 119.3$ Å. With two *PjAT* monomers of 50 kDa in the asymmetric unit, the V_M is 2.9 Å^3·Da^{-1} [63] with a calculated solvent content of 57%. A summary of data collection statistics is given in Table S1.

Using the FFAS03 server [64] and SCWRL [65], a homology model for *PjAT* was generated. Molecular replacement was performed with PHASER [66]. PHENIX PHASE and BUILD [67] was used for automatic building and COOT [68] was used for manual rebuilding and map inspection. The model was refined with REFMAC5 [69] with local NCS restraints and with TLS rigid body refinement as the last step, resulting in a final model comprising 2 protein molecules forming a homodimer. No significant conformational changes are observed between native and ligand-bound enzymes. The Cα atoms of all five models superimpose with root mean square deviations of 0.1–0.2 Å. The quality of the models was analyzed with MOLPROBITY [70]. Figures were prepared with PYMOL [71] and ESPRIPT [72].

Phylogenetic analyses

The sequences of several transaminases present in the PDB database were structurally aligned using the ProMals3D webserver (http://prodata.swmed.edu/promals3d). The multiple sequence alignment was provided to the MEGA X

software to perform evolutionary analyses with default settings [73].

Accession numbers

Atomic coordinates and experimental structure factor amplitudes are accessible at the protein databank (https://www.rcsb.org/) as entries 6G4B (E•succinate complex), 6G4C (E•phosphate complex), 6G4D (E•PLP complex), 6G4E (E•PLP•6-aminohexanoate complex), and 6G4F (E•PMP complex).

Acknowledgements

This work was supported by the Dutch Ministry of Economic Affairs through BE-Basic, grant FS02.005. CMP was supported by Erasmus Mundus, Eurotango II. QM was supported by the Chinese Scholarship Council.

Conflict of Interest

The authors declare no conflict of interest.

Author contributions

All authors designed experiments and contributed to the interpretation of the data. CMP cloned and isolated the enzyme. CMP and QM performed kinetic experiments and HJR solved the crystal structures. CMP, HJR, MO, and DBJ wrote the manuscript.

References

1 Dahlhoff G, Niederer JPM & Hoelderich WF (2001) ϵ-Caprolactam: new by-product free synthesis routes. *Catal Rev Sci Eng* **43**, 381–441.
2 Hong J & Xu X (2012) Environmental impact assessment of caprolactam production – a case study in China. *J Clean Prod* **27**, 103–108.
3 Andreoni V, Baggi G, Guaita C & Manfrin P (1993) Bacterial degradation of 6-aminocaproic acid polyamides (nylon 6) of low molecular weight. *Int Biodeterior Biodegradation* **31**, 41–53.
4 Wang CC & Lee CM (2007) Isolation of the ε-caprolactam denitrifying bacteria from a wastewater treatment system manufactured with acrylonitrile-butadiene-styrene resin. *J Hazard Mater* **145**, 136–141.
5 Hong S-J, Park G-S, Khan AR, Jung BK & Shin J-H (2016) Draft genome sequence of a caprolactam degrader bacterium: *Pseudomonas taiwanensis* strain SJ9. *Braz J Microbiol* **69**, 2015–2016.
6 Kulkarni RS & Kanekar PP (1998) Bioremediation of ε-caprolactam from nylon-6 waste water by use of *Pseudomonas aeruginosa* MCM B-407. *Curr Microbiol* **37**, 191–194.
7 Boronin AM, Naumova RP, Grishchenkov VG & Ilijinskaya ON (1984) Plasmids specifying ε-caprolactam degradation in *Pseudomonas* strains. *FEMS Microbiol Lett* **22**, 167–170.
8 Caspi R, Altman T, Billington R, Dreher K, Foerster H, Fulcher CA, Holland TA, Keseler IM, Kothari A, Kubo A *et al.* (2014) The MetaCyc database of metabolic pathways and enzymes and the BioCyc collection of pathway/genome databases. *Nucleic Acids Res* **42**, 459–471.
9 Takehara I, Fujii T, Tanimoto Y, Kato DI, Takeo M & Negoro S (2018) Metabolic pathway of 6-aminohexanoate in the nylon oligomer-degrading bacterium *Arthrobacter* sp. KI72: identification of the enzymes responsible for the conversion of 6-aminohexanoate to adipate. *Appl Microbiol Biotechnol* **102**, 801–814.
10 Otzen M, Palacio C & Janssen DB (2018) Characterization of the caprolactam degradation pathway in *Pseudomonas jessenii* using mass spectrometry-based proteomics. *Appl Microbiol Biotechnol* **102**, 6699–6711.
11 John RA (1995) Pyridoxal phosphate-dependent enzymes. *Biochim Biophys Acta* **1248**, 81–96.
12 Eliot AC & Kirsch JF (2004) Pyridoxal phosphate enzymes: mechanistic, structural, and evolutionary considerations. *Annu Rev Biochem* **73**, 383–415.
13 Mehta PK, Hale TI & Christen P (1993) Aminotransferases: demonstration of homology and division into evolutionary subgroups. *Eur J Biochem* **214**, 549–561.
14 Schneider G, Käck H & Lindqvist Y (2000) The manifold of vitamin B6 dependent enzymes. *Structure* **8**, R1–R6.
15 Schiroli D & Peracchi A (2015) A subfamily of PLP-dependent enzymes specialized in handling terminal amines. *Biochim Biophys Acta* **1854**, 1200–1211.
16 Höhne M, Schätzle S, Jochens H, Robins K & Bornscheuer UT (2010) Rational assignment of key motifs for function guides in silico enzyme identification. *Nat Chem Biol* **6**, 807–813.
17 Kirsch JF, Eichele G, Ford GC, Vincent MG, Jansonius JN, Gehring H & Christen P (1984) Mechanism of action of aspartate aminotransferase proposed on the basis of its spatial structure. *J Mol Biol* **174**, 497–525.
18 Crismaru CG, Wybenga GG, Szymanski W, Wijma HJ, Wu B, Bartsch S, de Wildeman S, Poelarends GJ, Feringa BL, Dijkstra BW *et al.* (2013) Biochemical properties and crystal structure of a β-phenylalanine

aminotransferase from *Variovorax paradoxus*. *Appl Environ Microbiol* **79**, 185–195.
19 Rudat J, Brucher BR & Syldatk C (2012) Transaminases for the synthesis of enantiopure beta-amino acids. *AMB Express* **2**, 11.
20 Shin J & Kim B (1999) Asymmetric synthesis of chiral amines with ω-transaminase. *Biotechnol Bioeng* **65**, 206–211.
21 Shin J-S, Yun H, Jang J-W, Park I & Kim B-G (2003) Purification, characterization, and molecular cloning of a novel amine:pyruvate transaminase from *Vibrio fluvialis* JS17. *Appl Microbiol Biotechnol* **61**, 463–471.
22 Kaulmann U, Smithies K, Smith MEB, Hailes HC & Ward JM (2007) Substrate spectrum of ω-transaminase from *Chromobacterium violaceum* DSM30191 and its potential for biocatalysis. *Enzyme Microb Technol* **41**, 628–637.
23 Rausch C, Lerchner A, Schiefner A & Skerra A (2013) Crystal structure of the ω-aminotransferase from *Paracoccus denitrificans* and its phylogenetic relationship with other class III aminotransferases that have biotechnological potential. *Proteins* **81**, 774–787.
24 Han S-W, Kim J, Cho H-S & Shin J-S (2017) Active site engineering of ω-transaminase guided by docking orientation analysis and virtual activity screening. *ACS Catal* **7**, 3752–3762.
25 Sayer C, Martinez-Torres RJ, Richter N, Isupov MN, Hailes HC, Littlechild JA & Ward JM (2014) The substrate specificity, enantioselectivity and structure of the (*R*)-selective amine:pyruvate transaminase from *Nectria haematococca*. *FEBS J* **281**, 2240–2253.
26 Pavkov-Keller T, Strohmeier GA, Diepold M, Peeters W, Smeets N, Schürmann M, Gruber K, Schwab H & Steiner K (2016) Discovery and structural characterisation new fold type IV-transaminases exemplify the diversity of this enzyme fold. *Sci Rep* **6**, 38183.
27 Kohls H, Steffen-Munsberg F & Höhne M (2014) Recent achievements in developing the biocatalytic toolbox for chiral amine synthesis. *Curr Opin Chem Biol* **19**, 180–192.
28 Slabu I, Galman JL, Lloyd RC & Turner NJ (2017) Discovery, engineering, and synthetic application of transaminase biocatalysts. *ACS Catal* **7**, 8263–8284.
29 Patil MD, Grogan G, Bommarius A & Yun H (2018) Recent advances in ω-transaminase-mediated biocatalysis for the enantioselective synthesis chiral amines. *Catalysts* **8**, 254.
30 Kelly SA, Pohle S, Wharry S, Mix S, Allen CCR, Moody TS & Gilmore BF (2018) Application of ω-transaminases in the pharmaceutical industry. *Chem Rev* **118**, 349–367.
31 Dunn PJ (2012) The importance of green chemistry in process research and development. *Chem Soc Rev* **41**, 1452–1461.
32 Palacio CM, Crismaru CG, Bartsch S, Navickas V, Ditrich K, Breuer M, Abu R, Woodley J, Baldenius K, Wu B *et al*. (2016) Enzymatic network for production of ether amines from alcohols. *Biotechnol Bioeng* **113**, 1853–1861.
33 Klatte S & Wendisch VF (2015) Role of L-alanine for redox self-sufficient amination of alcohols. *Microb Cell Fact* **14**, 9.
34 Turk SCHJ, Kloosterman WP, Ninaber DK, Kolen KPAM, Knutova J, Suir E, Schürmann M, Raemakers-Franken PC, Müller M, De Wildeman SMA *et al*. (2016) Metabolic engineering toward sustainable production of nylon-6. *ACS Synth Biol* **5**, 65–73.
35 Eaton MP (2008) Antifibrinolytic therapy in surgery for congenital heart disease. *Anesth Analg* **106**, 1087–1100.
36 Ager DJ, Li T, Pantaleone DP, Senkpeil RF, Taylor PP & Fotheringham IG (2001) Novel biosynthetic routes to non-proteinogenic amino acids as chiral pharmaceutical intermediates. *J Mol Catal B Enzym* **11**, 199–205.
37 Bommarius AS, Schwarm M & Drauz K (1998) Biocatalysis to amino acid-based chiral pharmaceuticals – examples and perspectives. *J Mol Catal B Enzym* **5**, 1–11.
38 Shin JS & Kim BG (1998) Kinetic modeling of omega-transamination for enzymatic kinetic resolution of α-methylbenzylamine. *Biotechnol Bioeng* **60**, 534–540.
39 Shin J & Kim B (2002) Exploring the active site of amine: pyruvate aminotransferase on the basis of the substrate structure – reactivity relationship: How the enzyme controls substrate specificity and stereoselectivity. *J Org Chem* **67**, 2848–2853.
40 Kim J, Kyung D, Yun H, Cho BK, Seo JH, Cha M & Kim BG (2007) Cloning and characterization of a novel β-transaminase from *Mesorhizobium* sp. strain LUK: a new biocatalyst for the synthesis of enantiomerically pure β-amino acids. *Appl Environ Microbiol* **73**, 1772–1782.
41 Shin JS & Kim BG (2001) Comparison of the ω-transaminases from different microorganisms and application to production of chiral amines. *Biosci Biotechnol Biochem* **65**, 1782–1788.
42 Sayer C, Isupov MN, Westlake A & Littlechild JA (2013) Structural studies of *Pseudomonas* and *Chromobacterium* ω-aminotransferases provide insights into their differing substrate specificity. *Acta Crystallogr D* **69**, 564–576.
43 Denesyuk AI, Denessiouk KA, Korpela T, Johnson MS & Akademi È (2002) Functional attributes of the phosphate group binding cup of pyridoxal phosphate-dependent enzymes. *J Mol Biol* **316**, 155–172.
44 Humble MS, Cassimjee KE, Hãkansson M, Kimbung YR, Walse B, Abedi V, Federsel HJ, Berglund P & Logan DT (2012) Crystal structures of the *Chromobacterium violaceum* ω-transaminase reveal

major structural rearrangements upon binding of coenzyme PLP. *FEBS J* **279**, 779–792.
45 Humble MS, Cassimjee KE, Abedi V, Federsel H-J & Berglund P (2012) Key amino acid residues for reversed or improved enantiospecificity of an ω-transaminase. *ChemCatChem* **4**, 1167–1172.
46 Liu W, Peterson PE, Carter RJ, Zhou X, Langston JA, Fisher AJ & Toney MD (2004) Crystal structures of unbound and aminooxyacetate-bound *Escherichia coli* gamma-aminobutyrate aminotransferase. *Biochemistry* **43**, 10896–10905.
47 Markova M, Peneff C, Hewlins MJ, Schirmer T & John RA (2005) Determinants of substrate specificity in omega-aminotransferases. *J Biol Chem* **280**, 36409–36416.
48 Wybenga GG, Crismaru CG, Janssen DB & Dijkstra BW (2012) Structural determinants of the β-selectivity of a bacterial aminotransferase. *J Biol Chem* **287**, 28495–28502.
49 Tripathi SM & Ramachandran R (2006) Direct evidence for a glutamate switch necessary for substrate recognition: crystal structures of lysine epsilon-aminotransferase (Rv3290c) from *Mycobacterium tuberculosis* H37Rv. *J Mol Biol* **362**, 877–886.
50 Tripathi SM, Agarwal A & Ramachandran R (2015) Mutational analysis of *Mycobacterium tuberculosis* lysine ε-aminotransferase and inhibitor co-crystal structures reveals distinct binding modes. *Biochem Biophys Res Commun* **463**, 154–160.
51 Marković-Housley Z, Schirmer T, Hohenester E, Khomutov AR, Khomutov RM, Karpeisky MY, Sandmeier E, Christen P & Jansonius JN (1996) Crystal structures and solution studies of oxime adducts of mitochondrial aspartate aminotransferase. *Eur J Biochem* **236**, 1025–1032.
52 Cho B, Park H-Y, Seo J-H, Kim J, Kang T-J, Lee B-S & Kim B-G (2008) Redesigning the substrate specificity of ω-aminotransferase for the kinetic resolution of aliphatic chiral amines. *Biotechnol Bioeng* **99**, 275–284.
53 Midelfort KS, Kumar R, Han S, Karmilowicz MJ, McConnell K, Gehlhaar DK, Mistry A, Chang JS, Anderson M, Villalobos A *et al.* (2013) Redesigning and characterizing the substrate specificity and activity of *Vibrio fluvialis* aminotransferase for the synthesis of imagabalin. *Protein Eng Des Sel* **26**, 25–33.
54 Genz M, Melse O, Schmidt S, Vickers C, Dörr M, van den Bergh T, Joosten H-J & Bornscheuer UT (2016) Engineering the amine transaminase from *Vibrio fluvialis* towards branched-chain substrates. *ChemCatChem* **8**, 1–5.
55 Nobili A, Steffen-Munsberg F, Kohls H, Trentin I, Schulzke C, Höhne M & Bornscheuer UT (2015) Engineering the active site of the amine transaminase from *Vibrio fluvialis* for the asymmetric synthesis of aryl-alkyl amines and amino alcohols. *ChemCatChem* **7**, 757–760.
56 Skalden L, Peters C, Dickerhoff J, Nobili A, Joosten HJ, Weisz K, Höhne M & Bornscheuer UT (2015) Two subtle amino acid changes in a transaminase substantially enhance or invert enantiopreference in cascade syntheses. *ChemBioChem* **16**, 1041–1045.
57 Steffen-Munsberg F, Vickers C, Thontowi A, Schätzle S, Meinhardt T, Svedendahl Humble M, Land H, Berglund P, Bornscheuer UT & Höhne M (2013) Revealing the structural basis of promiscuous amine transaminase activity. *ChemCatChem* **5**, 154–157.
58 Cassimjee KE, Humble MS, Land H, Abedib V & Berglund P (2012) *Chromobacterium violaceum* ω-transaminase variant Trp60Cys shows increased specificity for (S)-1-phenylethylamine and 4′-substituted acetophenones, and follows Swain-Lupton parameterisation. *Org Biomol Chem* **10**, 5466–5470.
59 Bouet A, Oudeyer S, Dupas G, Marsais F & Levacher V (2008) New advances in stereoselective Meyers' lactamization. Application to the diastereoselective synthesis of β-substituted oxazoloazepinones. *Tetrahedron: Asymmetry* **19**, 2396–2401.
60 Barber JEB, Damry AM, Calderini GF, Walton CJW & Chica RA (2014) Continuous colorimetric screening assay for detection of D-amino acid aminotransferase mutants displaying altered substrate specificity. *Anal Biochem* **463**, 23–30.
61 Kabsch W (2010) Integration, scaling, space-group assignment and post-refinement. *Acta Crystallogr D* 133–144.
62 Winn MD, Charles C, Cowtan KD, Dodson EJ, Leslie AGW, McCoy A, Stuart J, Garib N, Powell HR & Randy J (2011) Overview of the CCP 4 suite and current developments. *Acta Crystallogr D* **4449**, 235–242.
63 Matthews BW (1968) Solvent content of protein. *J Mol Biol* **33**, 491–497.
64 Jaroszewski L, Rychlewski L, Li Z, Li W, Godzik A, Program B, Road NTP & Jolla L (2005) FFAS03: a server for profile–profile sequence alignments. *Nucleic Acids Res* **33**, 284–288.
65 Canutescu AA, Shelenkov AA & Dunbrack RL Jr (2003) A graph-theory algorithm for rapid protein side-chain prediction. *Protein Sci* **12**, 2001–2014.
66 McCoy AJ, Grosse-Kunstleve RW, Adams PD, Winn MD, Storoni LC & Read RJ (2007) Phaser crystallographic software. *J Appl Crystallogr* **40**, 658–674.
67 Adams PD, Afonine PV, Bunkóczi G, Chen VB, Davis IW, Echols N, Headd JJ, Hung LW, Kapral GJ, Grosse-Kunstleve RW *et al.* (2010) PHENIX: a comprehensive Python-based system for macromolecular structure solution. *Acta Crystallogr D* **66**, 213–221.

68 Emsley P, Lohkamp B, Scott WG & Cowtan K (2010) Features and development of Coot. *Acta Crystallogr D* **66**, 486–501.
69 Murshudov GN, Skubák P, Lebedev AA, Pannu NS, Steiner RA, Nicholls RA, Winn MD, Long F & Vagin AA (2011) REFMAC 5 for the refinement of macromolecular crystal structures. *Acta Crystallogr D* **67**, 355–367.
70 Chen VB, Arendall WB III, Headd JJ, Keedy DA, Immormino RM, Kapral GJ, Murray LW, Richardson JS & Richardson DC (2010) MolProbity: all-atom structure validation for macromolecular crystallography. *Acta Crystallogr D* **66**, 12–21.
71 Delano WL (2002) Unraveling hot spots in binding interfaces: progress and challenges. *Curr Opin Struct Biol* **12**, 14–20.
72 Robert X & Gouet P (2014) Deciphering key features in protein structures with the new ENDscript server. *Nucleic Acids Res* **42**, W320–W324.
73 Kumar S, Stecher G, Li M, Knyaz C & Tamura K (2018) MEGA X: molecular evolutionary genetics analysis across computing platforms. *Mol Biol Evol* **35**, 1547–1549.
74 Kinoshita S, Negoro S, Muramatsu M, Bisaria VS, Sawada S & Okada H (1977) 6-Aminohexanoic acid cyclic dimer hydrolase. A new cyclic amide hydrolase produced by *Achromobacter guttatus* KI74. *Eur J Biochem* **80**, 489–495.
75 Kinoshita S, Terada T, Taniguchi T, Takene Y, Masuda S, Matsunaga N & Okada H (1981) Purification and characterization of 6-aminohexanoic-acid-oligomer hydrolase of *Flavobacterium* sp. K172. *Eur J Biochem* **116**, 547–551.

Supporting information

Additional supporting information may be found online in the Supporting Information section at the end of the article.

Table S1. Crystallographic data collection and refinement statistics.
Table S2. Class II/III TAs used for phylogenic analysis and groups interacting with substrate.
Fig. S1. Phylogenic analysis of transaminases.
Fig. S2. Crystal structure of PjAT and aspartate aminotransferase.